Table 2 Bending moments for optimized beams (in.-lb)

		Single-load case (load I = $M_A + M_B$)		Multiple-load case (load I = M_A, load II = M_B)	
		Unprestressed	Prestressed	Unprestressed	Prestressed
Initial	M_{a0}	...	0	...	0
	M_{b0}	...	707	...	7,202
	$M_{b'0}$	...	−707	...	−7,202
Initial + Load I	M_{a1}	15,000[a]	15,000[a]	15,000[a]	15,000[a]
	M_{b1}	14,338	15,000[a]	6,488	13,402
	$M_{b'1}$	30,662[b]	30,000[b]	−6,488	−13,402
Initial + Load II	M_{a2}	...	...	0	0
	M_{b2}	...	...	6,072	15,000[a]
	$M_{b'2}$	...	...	38,928[b]	30,000[b]

[a] Denotes $\max_j |M_{1j}|$ or $\max_j \{ |M_{10}|; |M_{10}+M_{1j}| \}$.

[b] Denotes $\max_j |M_{2j}|$ or $\max_j \{ |M_{20}|; |M_{20}+M_{2j}| \}$.

where $|M_{i0}|$ is the largest magnitude of initial moment in element i (i.e., in the unloaded prestressed structure), and $|M_{i0}+M_{ij}|$ is now the largest magnitude of moment in element i under load condition j. Thus, the M_{i0} are implicit functions of both X and X_p, whereas the M_{ij} remain implicit functions of X only, as previously.

Examples

Figure 2 shows a two-span beam which has been optimized in previous studies.[2,3] The beam is reconsidered here for optimization, utilizing initial element deformations as a prestressing mechanism. As in previous examples,[3] computations are based on the assumption that the elements have symmetric I-beam cross sections, and on assigned values $M_A = 15{,}000$ in.-lb, $L = 40$ in., yield stress = 30,000 psi, Young's modulus = 30×10^6 psi, material density = 0.3 lb/in.^{3}, and appropriate flange and web buckling relations.[3]

Results, and comparisons with the previous unprestressed designs, are presented in Table 1. Note that two distinct sets of designs are presented: one set for M_A and M_B applied simultaneously ("single-load" case), and one set for M_A and M_B applied independently ("multiple-load" case). Also note that only one independent initial deformation variable may be chosen in these examples. In order to maintain consistency with Fig. 1 and Eqs. (2), this variable may be taken as either the displacement or slope at the right end of element AB or the displacement at C of element BC. Table 1 shows equivalent optimum values of the first two of these alternate variables. It may be seen that the magnitudes of these variables are relatively small.

For both load cases, the inclusion of prestressing has resulted in weights lower than those of the unprestressed designs. This improvement is particularly significant in the multiple-load case, where the reduction is approximately 8%. This is also noteworthy in view of the fact that the unprestressed structure is inherently fully stressed,[‡] as are all optimum designs composed of this class of elements. It is thus apparent that the prestress leads to alternate, superior, fully stressed designs.

Table 2 illustrates the basis for the weight reductions by displaying the effects of initial deformations on the moment distributions in the optimized beams. Note that, in both load cases, the prestress leads to a reduction in the maximum moment in element 2 and to an equality of moment magnitudes at the ends of element 1. Thus, the moments in element 1, in essence, have been made as uniform as is possible under these load conditions.

It also may be noted that the maximum moments in elements 1 and 2 are now virtually identical in both the single and multiply loaded prestressed beams, which implies that the optimum designs also should be identical. This is confirmed in Table 1, which reflects only minor computational differences in the final designs.

In conclusion, it appears that prestressing by initial deformations is a factor deserving of additional consideration in beam structures as well as in truss structures. Such prestressing can provide significant reductions in weights of optimized structures; alternatively, it also is possible that relatively small but unintentional initial deformations of the type considered herein may degrade the integrity of structures which are optimized without consideration of initial stresses.

[‡] Fully stressed, in this context, is taken to mean that each element is constrained actively under at least one of the load conditions, such that simultaneous flange and web buckling is precluded; consequently, maximum stresses may be different for each element.

References

[1] Hofmeister, L. D. and Felton, L. P., "Prestressing in Structural Synthesis," *AIAA Journal*, Vol. 8, Feb. 1970, pp. 363-364.

[2] Felton, L. P. and Nelson, R. B., "Optimized Components in Frame Synthesis," *AIAA Journal*, Vol. 9, June 1971, pp. 1027-1031.

[3] Nelson, R. B. and Felton, L. P., "Thin-Walled Beams in Frame Synthesis," *AIAA Journal*, Vol. 10, Dec. 1972, pp. 1565-1569.

Some Effects of Combustion on Turbulent Mixing

Louis H. Bangert*
Georgia Institute of Technology, Atlanta, Ga.
and
Daniel I. Sebacher†
NASA Langley Research Center, Hampton, Va.

Introduction

MIXING and reacting compressible and turbulent flows play an important role in supersonic combustion propulsion systems. A question that has arisen in the past is

Received August 19, 1975; revision received November 10, 1975. Sponsored by the National Aeronautics and Space Administration under Grant NGR 11-002-177.

Index categories: Combustion in Gases; Airbreathing Propulsion, Hypersonic.

*Associate Professor, School of Aerospace Engineering. Member AIAA.

†Aerospace Technologist, High-Speed Aeronautics Division, Engine Performance Section.

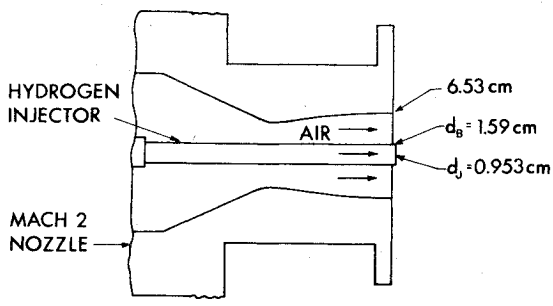

Fig. 1 Sketch of flow apparatus.

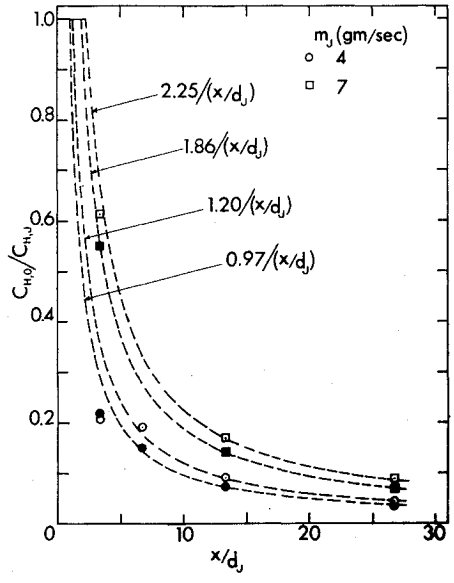

Fig. 2 Axial variation of mass fraction of hydrogen atoms. Open symbols: H_2-air. Closed symbols: H_2-N_2.

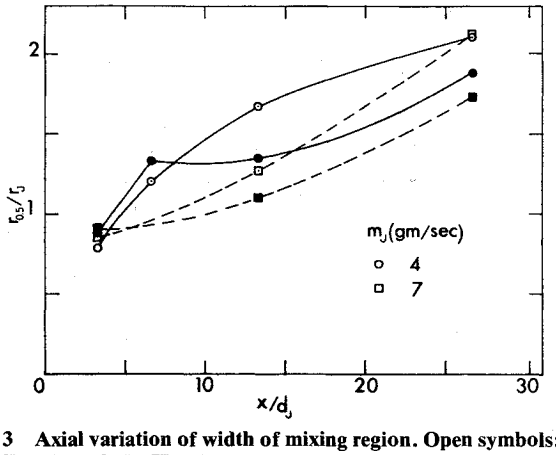

Fig. 3 Axial variation of width of mixing region. Open symbols: H_2-air. Closed symbols: H_2-N_2.

whether combustion affects turbulent mixing of the fuel and air streams. This question was considered by Cohen and Guile[1] in an investigation of coaxial hydrogen injection into vitiated air and nitrogen. They did not find an effect of chemical reaction on mixing rates for the conditions of their experiments. Beach[2] also studied coaxial hydrogen injection into air and nitrogen. His calculations indicated that the nonreacting nitrogen and hydrogen streams had a higher rate of mixing. No concentration measurements were made in this study, however, so no definite conclusions about relative mixing rates could be drawn. There have also been related studies of turbulent diffusion flames at low subsonic speeds. These studies, which produced conflicting evidence on the effect of combustion on mixing, have been summarized by Chigier and Strokin.[3] Chigier and Strokin also made detailed measurements in a round methane jet issuing into stagnant room temperature air. They found that near the nozzle, the diffusion coefficient (m^2/sec) in the flame was much less than for the corresponding cold jet. Farther downstream this condition was reversed, with the diffusion coefficient for the flame becoming larger.

The present study is concerned with mixing and combustion of near-sonic central hydrogen jets and coaxial supersonic air or nitrogen streams. Results of concentration measurements in these flows are presented.

Experimental Apparatus

The experiments were conducted in the Ceramic-Heated Tunnel[4] at NASA Langley Research Center. In this facility the test gas, air or nitrogen, is heated to a maximum stagnation temperature of 2220 K by passing it through a heated zirconia pebble bed. The test gas is then accelerated to Mach 1.98 in a stainless-steel, water-cooled nozzle with exit diameter 6.53 cm. The exit static pressure is 1.0 atm.

A hydrogen injector was mounted along the nozzle axis, as shown in Fig. 1. This injector is made from Inconel tubing 1.59 = cm o.d. and 0.89 = mm wall thickness. The injector also has a converging nozzle insert, so that the ratio of fuel jet to base diameter d_J/d_B is 0.60. Hydrogen entered the system at ambient temperature, and was heated as it cooled the injector walls. The hydrogen mass flow rate was measured by means of a calibrated orifice plate in the hydrogen supply line. The air and hydrogen jets exhausted into quiescent atmospheric air. For these flow conditions and the geometry shown in Fig. 1, the freestream air velocity U_e was 1,440 m/sec. Hydrogen mass flow rates of 4 and 7 g/sec were used in the experiments. These gave jet to freestream mass flux ratios $\rho_J U_J/\rho_e U_e$ of 0.15 and 0.27, respectively. The respective velocity ratios U_J/U_e were approximately 1.1 and 1.0.

The gas sampling probe is an 18° half-wedge, water-cooled, 4.76 = cm wide, and 1.03 = cm maximum thickness. Gas samples were withdrawn through nine ports, each 0.508 mm diam. These ports are on one face of the wedge, in a row perpendicular to the flow direction, 1.59 cm from the leading edge. They are equally spaced at 2.38 mm. A discussion of the use of this type of probe is given in Ref. 5. The gas samples were analyzed using a gas chromatograph.

Comparison of the mixing of the H_2-air and H_2-N_2 flows was made on the basis of the mean mass fraction of hydrogen atoms C_H. This quantity gives a measure of the amount of hydrogen present at a point, whether or not chemical reaction has taken place. The gas chromatograph analysis gave the mole fractions of H_2, O_2, and N_2 in the gas sample. To compute the corresponding mole fraction of H_2O, it was assumed that nitrogen and oxygen atoms at a point were in the same proportion as in air. The number of oxygen atoms computed in this way from the N_2 mole fraction, minus the number from the O_2 mole fraction, was the number that had gone into the formation of water.

Results

Figure 2 shows the variation of $C_{H,O}/C_{H,J}$ with x/d_J. Here $C_{H,O}$ is the value of C_H on the centerline, $C_{H,J} = 1$ is the value of C_H at the hydrogen jet exit, and x is the axial distance from the hydrogen jet exit. For both hydrogen flow rates, and for either air or N_2 as the freestream, $C_{H,O}/C_{H,J}$ was closely proportional to $(x/d_J)^{-1}$. Also, $C_{H,O}/C_{H,J}$ was larger for the burning hydrogen-air flows. Similar behavior was found by Chigier and Strokin.[3] The data at $\dot{m}_J = 4$ g/sec and $x/d_J = 3.3$ did not follow these trends, however. A definite explanation for this has not been found. It may also be noted that the values of $C_{H,O}/C_{H,J}$ scale almost exactly with $\dot{m}_J$ for these data.

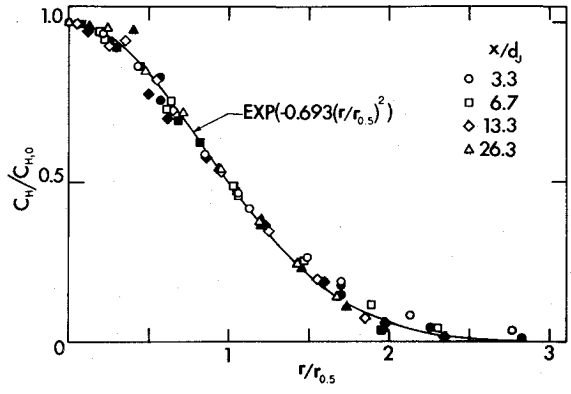

Fig. 4 Radial profiles of mass fraction of hydrogen atoms for $\dot{m}_J = 4$ g/sec. Open symbols: H_2-air. Closed symbols: H_2-N_2.

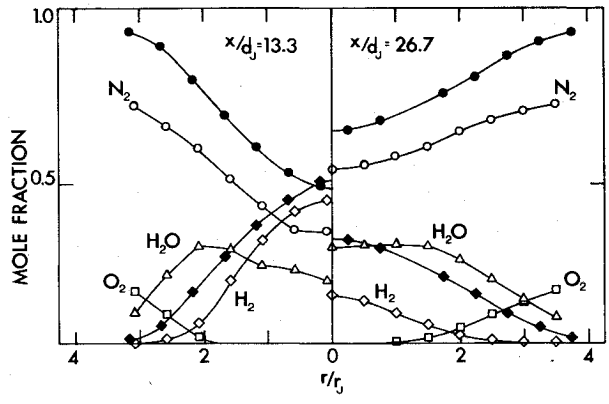

Fig. 5 Sample radial profiles of specie mole fractions for $\dot{m}_J = 4$ g/sec. Open symbols: H_2-air. Closed symbols: H_2-N_2.

In Fig. 3 the variation of the nondimensional width of the mixing region, $r_{0.5}/r_J$, is shown. Here, $r_{0.5}$ the distance from the axis at which $C_H/C_{H,O} = 0.5$, and $r_J = 0.5\, d_J$. The relative values of $r_{0.5}/r_J$ for combustion and no combustion are influenced by density differences, as well as by possible mixing rate differences. Thus, conclusions about relative mixing cannot be drawn directly from the data of Fig. 3. Because of the lack of temperature measurements, it was not possible to construct accurate mass-averaged profiles.

Figure 4 shows that the data for $C_H/C_{H,O}$ are well-described by a Gaussian profile when plotted against $r/r_{0.5}$. Essentially the same behavior was found for $\dot{m}_J = 7$ g/sec.

Flow field calculations were made to aid interpretation of the experimental data. These calculations used the time-average conservation equations for mass, momentum, energy, chemical species, mean-square fluctuation of mass fraction of O_2 and H_2, turbulence kinetic energy, and turbulence dissipation rate in the boundary-layer approximation. The correlations that appear in these equations were modeled as described by Launder and Spalding.[6,7] A reaction rate model for turbulent diffusion flames was also used.[8] These calculations were made for the same initial conditions as in the experiments, but with an infinitesimally thin injector wall. The numerical solution used a finite-difference method based on that of Patankar and Spalding.[9]

The calculated results for $C_{H,O}/C_{H,J}$ were similar to the experimental results shown in Fig. 2. Also, the calculated values of $r_{0.5}/r_J$ were larger with combustion. However, the turbulent mass transport coefficient (kg/m sec) and the mean density at $r_{0.5}$ were everywhere larger with no combustion. The turbulent diffusion coefficient (m^2/sec) with combustion was smaller near the injector, but then became larger a few injector diameters away. This latter behavior was also observed in the free-jet experiments of Chigier and Strokin.[3] Finally,

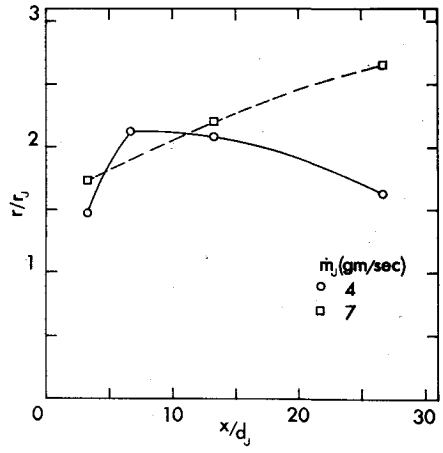

Fig. 6 Flame contours based on stoichiometric conditions.

the calculations showed larger turbulence kinetic energy with combustion, except very close to the injector. Similar results were also observed by Chigier and Strokin.[3]

These calculated results, plus the experimental results of Chigier and Strokin,[3] suggest the following interpretation of the data of Figs. 2 and 3. The turbulent diffusion coefficient (m^2/sec) becomes larger with combustion within a small distance from the hydrogen nozzle. The lower density of the flow with combustion produces lower mass transport coefficients (kg/m sec), however, leading to the results shown in Fig. 2. Also, the lower density of the flow with combustion seems responsible for the larger values of $r_{0.5}/r_J$ with combustion shown in Fig. 3.

Figures 5 and 6 provide additional information about the present experiments. Radial profiles of mole fractions at x/d_J of 13.3 and 26.7 for $\dot{m}_j = 4$ g/sec are shown in Fig. 5. Flame contours are shown in Fig. 6, based on the locations where the mean mole fractions of H_2 and O_2 are in stoichiometric proportions.

Conclusions

The present experiments for mixing and combustion of near-sonic central hydrogen jets with coaxial supersonic air or nitrogen streams have shown larger concentrations of hydrogen near the axis when there was combustion. Results of present flowfield calculations, and of low-speed free jet experiments,[3] suggest that this behavior was caused primarily by lower density in the burning case producing lower turbulent mass transport coefficients (kg/m sec).

References

[1] Cohen, L. S. and Guile, R. N., "Measurements in Freejet Mixing/Combustion Flow," *AIAA Journal*, Vol. 8, June 1970, pp. 1053-1061.

[2] Beach, H. L., Jr., "Supersonic Mixing and Combustion of a Hydrogen Jet in a Coaxial High Temperature Test Gas," AIAA Paper 72-1179, New Orleans, La., 1972.

[3] Chigier, N. A. and Strokin, V., "Mixing Processes in a Free Turbulent Diffusion Flame," *Combustion Science and Technology*, Vol. 9, 1974, pp. 111-118.

[4] Trout, O. F., Jr., "Design, Operation, and Testing Capabilities of the Langley 11-Inch Ceramic-Heated Tunnel," TN D-1598, 1963, NASA.

[5] Lengelle, G. and Vervier, C., "Gas Sampling and Analysis in Combustion Phenomena," AGARDograph 168, 1973, pp. 49-54.

[6] Launder, B. E. and Spalding, D. B., "The Numerical Computation of Turbulent Flow," *Computer Methods in Applied Mechanics and Engineering*, Vol. 3, March 1974, pp. 269-289.

[7] Spalding, D. B., "Concentration Fluctuations in a Round Turbulent Free Jet," *Chemical Engineering Science*, Vol. 26, 1971, pp. 95-107.

[8] Bangert, L. H., "Study of Effects of Injector Geometry on Fuel-Air Mixing and Combustion," NGR-11-002-177, March-August 1974, NASA Langley Research Center, Hampton, Va.

[9] Patankar, S. V. and Spalding, D. B., *Heat and Mass Transfer in Boundary Layers*, 2nd ed., International Textbook Co., London, 1970.